ISSN: 1410-8917
Jurnal Kimia Sains & Aplikasi
e-ISSN: 2597-9914

Jurnal Kimia Sains dan Aplikasi 26 (10) (2023): 404-410

Jurnal Kimia Sains dan Aplikasi
Journal of Scientific and Applied Chemistry

Journal homepage: http://ejournal.undip.ac.id/index.php/ksa

Synthesis and Characterization of Fe-doped Hydroxyapatite/ZnO Nanocomposites Using the Coprecipitation Method from Processed Limestone

Arie Hardian [1,*], Rosalinawati Dewi [1], Jasmansyah [1], Dani Gustaman Syarif [2], Anceu Murniati [1]

[1] Master of Chemistry Study Program, Faculty of Science and Informatics, Jenderal Achmad Yani University, Cimahi, Indonesia
[2] Center for Applied Nuclear Science and Technology (PSTNT)-Nuclear Energy Research Organization (ORTN)-National Innovation Research Agency (BRIN), Bandung, Indonesia

* Corresponding author: arie.hardian@lecture.unjani.ac.id

https://doi.org/10.14710/jksa.26.10.404-410

Article Info

Article history:

Received: 08th September 2023
Revised: 18th December 2023
Accepted: 20th December 2023
Online: 23rd December 2023

Keywords:
limestone; iron; doped hydroxyapatite; nanocomposites; zinc oxide

Abstract

Hydroxyapatite (HAp) is the main inorganic component that forms teeth and bones. The abundant limestone reservoir in Indonesia can be utilized as a natural resource for the green synthesis of hydroxyapatite. The objective of synthesizing Fe-doped hydroxyapatite/ZnO nanocomposites is to enhance the magnetic properties of hydroxyapatite, facilitating its utilization as a biomaterial in drug delivery systems. This application proves valuable in regulating the timing and location of active substance decay in pharmaceuticals. The coprecipitation method was employed to synthesize Fe-doped hydroxyapatite (Fe-HAp) at varying concentrations of 0%, 2.5%, 5%, and 10% mol. Subsequently, Fe- HAp/ZnO nanocomposites were crafted with a weight ratio 4:1 through straightforward homogenization between nano Fe-HAp and nano ZnO, utilizing ethanol as a solvent. The analytical tools employed for characterization included X-ray fluorescence (XRF), X-ray diffraction (XRD), and Vibrating Sample Magnetometer (VSM). XRF analysis revealed that the Ca/P ratio in the Fe- HAp/ZnO nanocomposite decreased with increasing Fe dopant concentration, while the weight percentage of ZnO remained consistent across all nanocomposites. The XRD results demonstrated the presence of typical diffraction patterns of HAp and ZnO in the Fe-HAp/ZnO nanocomposite. However, secondary phases such as β-TCP, $CaCO_3$, and Fe_2O_3 were observed in the Fe-HAp sample. The crystallite size of the Fe-HAp/ZnO nanocomposite generated in this study ranged from 29 to 38 nm. VSM characterization outcomes indicated that the substitution of Fe(III) can modify the diamagnetic properties of hydroxyapatite, rendering it ferromagnetic or superparamagnetic, depending on the dopant concentration employed.

1. Introduction

The current demand for robust implants and bone substitutes is driven by their attributes related to biocompatibility, bioactivity, and mechanical properties. The primary challenge faced by researchers is the prevention of immune rejection. Customization of bone replacement structures is essential, requiring meticulous control of microscopic details for each patient. Similarly, in drug carrier systems, effective control of drug release rate and duration, alongside addressing toxicity and side effects, presents significant challenges. Numerous endeavors have been undertaken to devise uncomplicated, efficient, and environmentally friendly methodologies for fabricating biomaterials with desirable biocompatibility, bioactivity, and robust mechanical properties. These biomaterials find applications in drug carrier systems as well [1]. Hydroxyapatite (HAp), the principal component responsible for bone and tooth formation, emerges as a highly suitable material for such

biomaterial development. Compounds falling under the apatite category are characterized by the chemical formula $M_{10}(XO_4)_6Z_2$, where M^{2+} represents a metal cation, XO_4^{3-} and Z^- denote anions. In pure HAp, M corresponds to Ca^{2+}, X to P^{5+}, and Z to OH^-, maintaining a Ca/P ratio of 1.67 [2]. The specific surface area and inherent properties of HAp play a crucial role, especially in biomedical applications. Consequently, nano-sized HAp (nano-HAp) with an exceptionally large specific surface area stands out as a superior candidate in the realm of biomaterial development for biomedical applications.

Pure nano-sized hydroxyapatite (nano-HAp) exhibits drawbacks, including suboptimal mechanical properties, challenges in bodily absorption, and limited bioactivity, particularly regarding antibacterial properties. To address these limitations, substituting Ca^{2+} ions in HAp with various other metal ions, such as Fe, Mg, Zn, Cd, La, Y, and others, has been explored [3, 4, 5, 6]. This substitution method is commonly referred to as doping, involving partial substitutions at specific ion positions without altering the crystal system. The effectiveness of the doping technique is discernible through X-ray diffraction analysis, where the diffraction pattern remains consistent, but a shift in the diffraction angle towards a smaller or larger direction is observed.

Nano-HAp doped with iron(III) ions (Fe-HAp) has been documented to yield advantages such as smaller particle sizes, enhanced mechanical and dielectric properties, heightened antibacterial efficacy, and prolonged drug release duration [7]. Furthermore, Tampieri *et al.* [8] reported that Fe-HAp exhibits superparamagnetic properties, rendering it suitable for applications in drug carrier systems, anti-cancer therapy, and bone surgery. A bioactive nanocrystalline hydroxyapatite powder doped with iron (Fe-doped n- HAp), featuring varying concentrations of Fe, was successfully synthesized using the reflux method. In antibacterial activity tests, Fe-doped n-HAp, when combined with the antibiotic amoxicillin, demonstrated significant inhibition against bacterial strains [7]. The high hyperthermia of Fe-HA presents distinct advantages in anti-cancer therapy, offering a more intense and rapid local effect. Importantly, its biocompatibility and degradability overcome the side effects associated with long-term cytotoxicity [8]. Jose *et al.* [7] was successfully synthesized Fe-HAp nanocrystals with Fe concentrations of 0.05, 0.1, and 0.2 M using the reflux method. A notable observation was the morphological change from spherical to needle-like crystals with increasing iron concentration. Fe doping at 0.1 and 0.2 M exhibited robust antibacterial activity against *E. coli* bacteria using the disk diffusion method. Predoi *et al.* [9] was reported the successful synthesis of Fe-HAp 0.05 M in suspension form using the coprecipitation method. Fe-HAp, produced in both suspension and coating forms, demonstrated commendable biocompatibility properties based on MTT analysis. Alizadeh and Salimi [10] was synthesized Fe-HAp by utilizing coal ash waste as a source of Fe^{3+} and Ca^{2+} cations through the precipitation method [10]. Subsequently, Shu *et al.* [11] was employed artificial converter slag processed by salicylic acid, a final product in steelmaking, as a source of Fe^{3+} and Ca^{2+} cations in the hydrothermal synthesis of Fe-Hap.

In the pursuit of sustainable nano-sized hydroxyapatite (nano-HAp)-based biomaterials, the utilization of natural calcium sources as nano-HAp precursors, including mammalian bones, marine biota, eggshells, plants, algae, and minerals, takes precedence [12]. Among the diverse natural sources of calcium, minerals like limestone exhibit substantial potential for the large-scale production of this HAp biomaterial.

Nanomedicine stands out as one of the rapidly advancing branches of nanotechnology, revolutionizing disease diagnosis and therapy at the cellular and molecular levels. Over the past decades, metal oxide nanoparticles have gained prominence in biology and medicine due to their distinctive physicochemical properties. Among these nanomaterials, zinc oxide nanoparticles (ZnO-NPs) have garnered significant attention from researchers for therapeutic and diagnostic applications owing to their low toxicity, biodegradability, and cost-effectiveness [13]. The amalgamation of ZnO and HAp proves intriguing in biomaterial development for biomedical applications. A study by Barua *et al.* [14] highlighted that ZnO has the potential to enhance the porosity, compressive strength, thermal stability, and swelling properties of frameworks. Additionally, incorporating ZnO at a concentration of 5% (w/w) demonstrated the ability to augment the bioactivity and biocompatibility properties of HAp composites.

The incorporation of composites has become imperative in the application of materials or biomaterials, owing to their ability to amalgamate the superior properties of each constituent. Consequently, the fabrication of composites involving Fe-HAp with ZnO emerges as a strategic approach to produce biomaterials with enhanced bioactivity, a crucial requirement in biomedical applications, particularly in drug carrier systems. Numerous investigations on implant materials based on HAp-ZnO composites have demonstrated superior compatibility and antimicrobial activity in vivo and in vitro. Furthermore, this composite has proven effective as a coating material for dental implants, exhibiting anti-biofilm activity, osteoblast mineralization, antimicrobial properties, bone tissue engineering, bone implantation, increased antibacterial activity, biocompatibility, bone restoration, sealing ability in endodontically treated teeth, and repair of bone defects [15].

This article aims to elucidate the potential of local Padalarang limestone minerals as a viable source of Ca^{2+} in the synthesis of nano Fe-HAp. It will delve into the methodology of varying the Fe concentration based on %mol $Ca_{10-x}Fe_x(PO_4)_6(OH)_{2+z}$, with x ranging from 0% to 10%. Additionally, this article will explore how the crystal characteristics, morphology, and magnetic profile of Fe- HAp/ZnO nanocomposites have not been reported previously.

2. Experimental

2.1. Tools and Materials

Various tools and instrumentations were employed, including glassware, a hot plate with a magnetic stirrer, an oven, a furnace, a mortar and pestle, an alumina crucible, a centrifuge, an X-ray Fluorescence Spectrophotometer (XRF) Bruker S8 Tiger, an X-ray Diffractometer (XRD) Bruker D8 Advance, and a Vibrating Sample Magnetometer (VSM).

The materials were processed limestone sourced from PT. Kurnia Artha Pratiwi, specified in Table 1, ZnO nanoparticles, $Fe(NO_3)_3.9H_2O$ (Merck, ≥99.95% trace metals basis), $(NH_4)_2HPO_4$ (Merck, ACS reagent, ≥98%), aluminum foil, and distilled water.

2.2. Extraction of *Hibiscus sabdariffa* Linn Petals

2.2.1. Synthesis and Characterization of Fe-doped HAp (Fe-HAp)

Calcium oxide (CaO) was initially made by calcinating limestones at 900°C for 5 hours. CaO and iron nitrate nonahydrate ($Fe(NO_3)_3.9H_2O$) were individually weighed by stoichiometry to generate nano-sized Fe- Hydroxyapatite (Fe-HAp) with varied Fe concentrations: 0% ($Ca_{10}(PO_4)_6(OH)_2$, HAp), 2.5% ($Ca_{9.75}Fe_{0.25}(PO_4)_6(OH)_{2.1}$, Fe2.5-HAp), 5% ($Ca_{9.5}Fe_{0.5}(PO_4)_6(OH)_{2.5}$, Fe5-HAp), and 10% ($Ca_9Fe(PO_4)_6(OH)_3$, Fe10-HAp). Subsequently, 100 mL of distilled water was added, and a 0.3 M $(NH_4)_2HPO_4$ solution was slowly introduced into the mixed suspension according to stoichiometry, with continuous stirring for approximately 90 minutes.

The mixture was then allowed to stand for 12 hours until complete sedimentation occurred. The resulting precipitate was filtered, separated using a centrifuge, and dried at 110°C for 3 hours. The obtained powder underwent calcination at 700°C for 3 hours. The calcined powder was subject to compositional analysis through the X-ray fluorescence (XRF) method and structural examination utilizing the X-ray diffraction (XRD) method.

2.2.2. Preparation of Fe-HAp/ZnO Composite

The Fe-Hydroxyapatite/Zinc Oxide (Fe-HAp/ZnO) nanocomposite was prepared by blending Fe-HAp nanopowder and ZnO nanopowder in a weight ratio of 4:1. Subsequently, ethanol was added to the mixture, which was homogenized for 90 minutes. The resulting blend was dried at room temperature for 12 hours, followed by filtration and subsequent drying at 110°C for 5 hours. The Fe-HAp/ZnO nanocomposite powder was subjected to characterization utilizing XRF, XRD, and a Vibrating Sample Magnetometer (VSM).

3. Results and Discussion

3.1. Elemental Composition Analysis

Based on the XRF analysis results presented in Table 2, it is evident that the Ca/P ratio of synthetic Fe- doped Hydroxyapatite/ZnO nanocomposites is comparatively smaller (ranging from 1.66 to 1.74) in contrast to the Ca/P ratio of nanohydroxyapatite (ranging from 1.81 to 1.84). This discrepancy allows for the potential formation of calcium compounds beyond hydroxyapatite, specifically Tri Calcium Phosphate (TCP). Previous research by Saryati *et al.* [16] calcining raw clam shells using a precipitation reaction also produced the peak phase of TCP and HAp phase with a calcination temperature of 700-1000°C which can be seen from the Ca/P ratio, which is greater than the Ca/P ratio of hydroxyapatite.

Other research states that the formation of TCP is attributed to the thermal treatment undertaken in the calcination process. In this process, carbon dioxide interacts with deionized water, generating carbonate anions (CO_3^{2-}), which are subsequently incorporated into the crystal lattice of HAp. Hydroxyapatite (HAp) undergoes decomposition, resulting in the formation of the tricalcium phosphate (TCP) phase, which is discernible at a temperature of 700°C and achieves complete crystallization beyond 900°C. TCP exhibits stability within the temperature range of 1200 to 1400°C [17]. Conversely, the weight percentage of zinc (Zn) remains relatively consistent across all samples, exhibiting no significant variance based on the initial stoichiometry.

Table 1. Specifications of Padalarang limestone mineral from PT. Kurnia Artha Pratiwi

Parameter	Unit	RHEOCARB 7	Method
$CaCO_3$	%	98.01	ASTM C 25-31
MgO	%	0.27	
Water content	%	0.29	ASTM C 25-20
Brightness R457/T525	%	88.33	ISO2470
MALVERN			
D 98	μ	8.05	Malvern Mastersizer 2000E-Laser Particle Size Analysis

Table 2. Elemental composition of Fe-HAp/ZnO composite based on XRF analysis

Sample	Composition (%w/w)				Composition (mol)			Ca/P	(Ca+Fe)/P
	Ca	P	Fe	Zn	Ca	P	Fe		
Limestones	97.34	-	0.5189	-	-	-	-	-	-
HAp	55.19	23.26	0.28	-	1.38	0.75	-	1.84	1.84
HAp/ZnO	45.77	19.43	0.17	33.51	1.14	0.63	-	1.81	1.81
Fe2.5-HAp/ZnO	43.03	19.31	2.31	34.17	1.08	0.62	0.04	1.74	1.81
Fe5-HAp/ZnO	41.02	19.26	4.76	33.62	1.03	0.62	0.09	1.66	1.81
Fe10-HAp/ZnO	39.2	18.38	8.86	32.57	0.98	0.59	0.16	1.66	1.93

Note: Limestone = processed limestone from PT. Kurnia Artha Pratiwi, Padalarang; HAp = HAp synthesized from limestone; HAp/ZnO = HAp and ZnO composite with a %w/w ratio of 4:1; Fe2.5-HAp/ZnO = HAp composite doped with 2.5%mol Fe and ZnO with a %w/w ratio of 4:1; Fe5-HAp/ZnO = HAp composite doped with 5 mol% Fe and ZnO with a %w/w ratio of 4:1; and Fe10-HAp/ZnO = HAp composite doped with 10 mol% Fe and ZnO with a %w/w ratio of 4:1.

3.2. Crystal Structure Analysis

Based on Figure 1, there are secondary phases in synthetic HAp, including β-TCP and $CaCO_3$. The presence of the side product β-TCP in the synthesis of HAp using the wet chemical method was also reported by Kaygili *et al.* [18] who synthesized HAp using the sol-gel method.

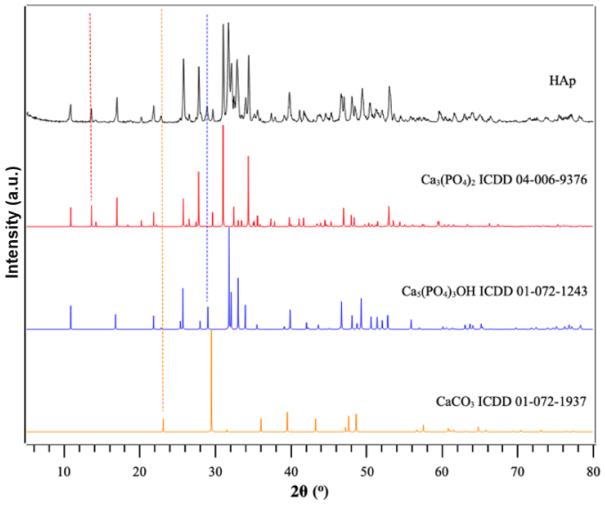

Figure 1. X-ray diffraction pattern of HAp synthesized from processed limestone compared to the ICDD database

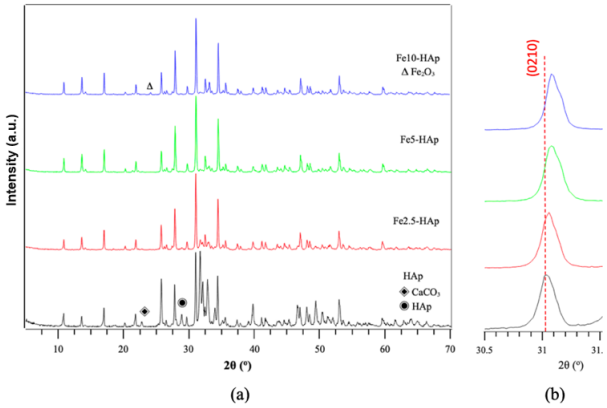

Figure 2. (a) X-ray diffraction patterns of HAp and Fe-HAp with various Fe dopant concentrations (2.5%, 5%, and 10% mol) and (b) magnification of the diffraction pattern in the (0210) plane for the β -TCP crystal

According to the findings presented in Figure 2a, it is evident that the introduction of Fe dopant exerts a suppressing influence on the formation of the calcite phase. Furthermore, as the concentration of Fe dopant increases, there is a noticeable reduction in the proportion of Hydroxyapatite (HAp) relative to β- Tricalcium Phosphate (β-TCP). Consequently, incorporating a higher dopant concentration, specifically at 10% mol, leads to the appearance of the secondary phase Fe_2O_3. In Figure 2b, the diffraction angle at 31.02° corresponding to the (0210) plane of the β-TCP crystal is observed to shift towards a larger 2θ. Following Bragg's law applicable to various crystal systems, a larger diffraction angle signifies a smaller distance between crystal planes and, consequently, a reduced unit cell size.

The reduction in unit cell size is attributed to the partial substitution of Ca^{2+} ions (1.12 Å) by Fe^{3+} ions (0.78 Å), which possess a smaller ion radius [19]. Hence, it can be concluded that the Fe dopant is successfully incorporated into the β-TCP crystal. The observed shift in the diffraction angle in HAp proves challenging to discern, given the very small relative intensity compared to the β-TCP phase.

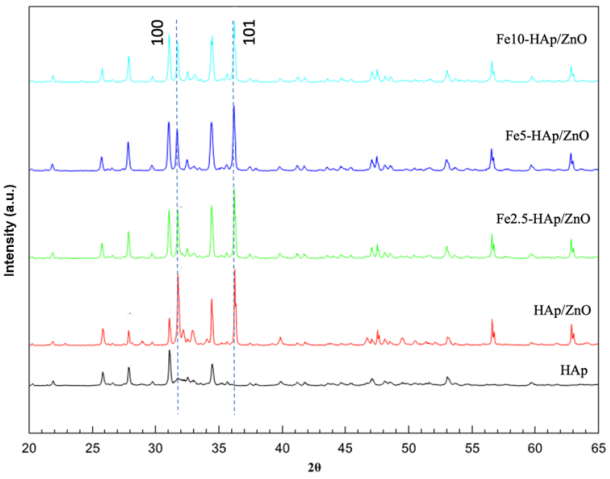

Figure 3. X-ray diffraction patterns of Fe-HAp and Fe- HAp/ZnO composites

Table 3. Fe-HAp/ZnO composite crystallite size obtained through Scherrer calculations

Sample	Average crystallite size (nm)
HAp	24
HAp/ZnO	29
Fe2.5-HAp/ZnO	37
Fe5-HAp/ZnO	36
Fe10-HAp/ZnO	38

Based on Figure 3, it is apparent that all composites exhibit additional diffraction peaks, signifying the presence of ZnO. Specifically, peaks are observed at angles of 32° for the (100) plane and 36.4° for the (101) plane, consistent with the JCPDS 36-1451 standard. This observation serves as an indication that the composite has been successfully formed. Conversely, the average crystallite size was calculated using the Scherrer equation approach (Equation 1) [20].

$$d = \frac{k.\lambda}{\beta.cos\theta} \quad (1)$$

The calculation of the crystallite size (d) was performed using Scherrer's equation (Equation 1), where k represents Scherrer's constant (0.9), λ denotes the wavelength of the X-ray Cu Kα (0.15406 nm), β signifies the full width at half maximum (FWHM) in radians, and θ represents the diffraction angle in radians at the five highest peaks, namely 28.02°, 31.09°, 32°, 34.5°, and 36.4°. The results of these calculations are presented in Table 3, revealing that the average crystallite size for both the HAp and nanocomposite samples falls within the range of 24-38 nm.

3.3. Magnetic Properties Analysis

According to the outcomes of the VSM analysis, illustrated in the M-H curve depicted in Figure 4, the HAp/ZnO sample exhibits a pattern consistent with diamagnetic materials (DM). The magnetic moment is inversely proportional to the applied magnetic field in diamagnetic materials. This observation indicates that both HAp and ZnO possess diamagnetic properties, a characteristic previously reported for HAp by Ateş *et al.* [21]. In contrast, the Fe2.5-HAp/ZnO nanocomposite demonstrates ferromagnetic (FM) properties at low magnetic fields (< 0.5 T), as indicated by the blue circle. Furthermore, Fe(III) dopant concentrations of 5% and 10% exhibit both ferromagnetic (FM) and superparamagnetic (SPM) properties. The magnetic properties of Fe-doped HAp have been previously documented by Silva *et al.* [22] and Fe-doped β-TCP was reported by Singh *et al.* [23].

The magnetic characteristics of the composite, as inferred from the M-H curve, are detailed in Table 4. Fe10-HAp/ZnO is categorically identified as a type of superparamagnetic material, given the residual magnetic value (M_r) proximity to 0. This finding aligns with the observations reported by Tampieri *et al.* [8], in which Fe- HAp was synthesized using the simultaneous addition method (T = 40°C) and oxidative method (T = 60°C), exhibiting the characteristic superparamagnetic M-H curve phenomenon.

Table 4. M_s, M_r, and H_c values for Fe-HAp/ZnO composite samples

Sample	Type	M_s (emu/g)	M_r (emu/g)	H_c (T)
HAp/ZnO	DM	-	-	-
Fe2.5-HAp/ZnO	DM/FM	-	-	-
Fe5-HAp/ZnO	FM	0.0451	0.0083	0.0341
Fe10-HAp/ZnO	SPM	0.0481	0.0001	0.0031

Note: M_s = magnetic saturation; M_r = residual magnetism; H_c = coercivity

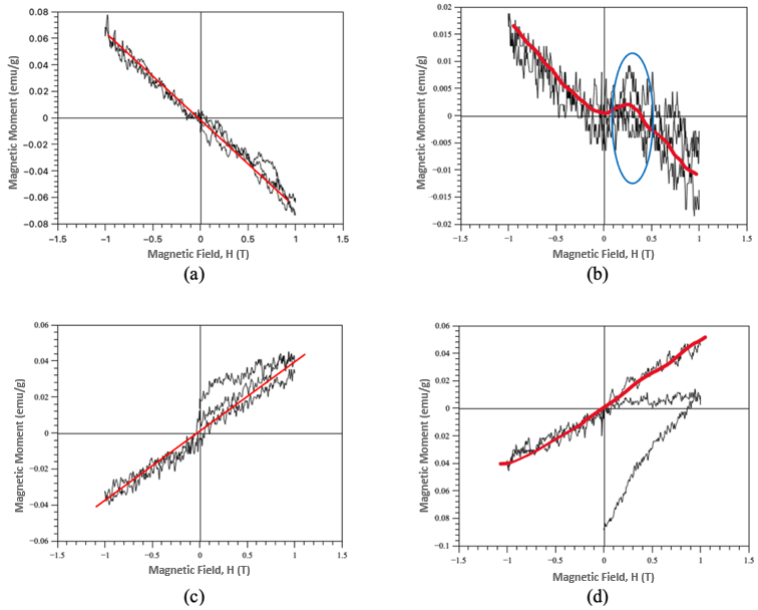

Figure 4. M-H curve of nanocomposite samples a) HAp/ZnO, b) Fe2.5-HAp/ZnO, c) Fe5-HAp/ZnO, and Fe10-HAp/ZnO. The red line shows the M-H pattern, and the blue circle indicates the appearance of ferromagnetic properties

4. Conclusion

The synthesis of Fe(III) doped hydroxyapatite (Fe- HAp) was effectively accomplished through the coprecipitation method utilizing locally processed limestone. The resultant hydroxyapatite retained secondary phases: β-TCP, $CaCO_3$, and Fe_2O_3. The average particle size of the resulting Fe-doped hydroxyapatite/ZnO nanocomposites falls within the nanometer scale (24-38 nm). Incorporating Fe(III) into hydroxyapatite crystals is a strategic approach capable of transforming the diamagnetic properties of hydroxyapatite into superparamagnetic characteristics.

Acknowledgments

This research was funded by a Postgraduate Program grant-Master's Thesis Research with number 180/E5/PG.02.00.PL/2023 and a General Achmad Yani University Internal Research Grant with number SKEP/194/UNJANI/VI/2023. The author would like to thank PT. Kurnia Artha Pratiwi, who has facilitated the processing of limestone materials. The author would also like to thank Mr. M. Yamin (BRIN), Istiqomah Triandini, and Vira Audry Premitha, who helped with the research.

References

[1] Aleksandra Szcześ, Lucyna Hołysz, Emil Chibowski, Synthesis of hydroxyapatite for biomedical applications, *Advances in Colloid and Interface Science*, 249, (2017), 321-330 https://doi.org/10.1016/j.cis.2017.04.007

[2] V. Sarath Chandra, Ganga Baskar, R. V. Suganthi, K. Elayaraja, M. I. Ahymah Joshy, W. Sofi Beaula, R. Mythili, Ganesh Venkatraman, S. Narayana Kalkura, Blood Compatibility of Iron-Doped Nanosize Hydroxyapatite and Its Drug Release, *ACS Applied Materials & Interfaces*, 4, 3, (2012), 1200-1210 https://doi.org/10.1021/am300140q

[3] Monika Šupová, Substituted hydroxyapatites for biomedical applications: A review, *Ceramics International*, 41, 8, (2015), 9203-9231 https://doi.org/10.1016/j.ceramint.2015.03.316

[4] A. Joseph Nathanael, D. Mangalaraj, S. I. Hong, Y. Masuda, Synthesis and in-depth analysis of highly ordered yttrium doped hydroxyapatite nanorods prepared by hydrothermal method and its mechanical analysis, *Materials Characterization*, 62, 12, (2011), 1109-1115 https://doi.org/10.1016/j.matchar.2011.09.008

[5] Vijay Kumar Mishra, Birendra Nath Bhattacharjee, Om Parkash, Devendra Kumar, Shyam Bahadur Rai, Mg-doped hydroxyapatite nanoplates for biomedical applications: A surfactant assisted microwave synthesis and spectroscopic investigations, *Journal of Alloys and Compounds*, 614, (2014), 283-288 https://doi.org/10.1016/j.jallcom.2014.06.082

[6] Zafer Evis, Bengi Yilmaz, Metin Usta, Salim Levent Aktug, X-ray investigation of sintered cadmium doped hydroxyapatites, *Ceramics International*, 39, 3, (2013), 2359-2363 https://doi.org/10.1016/j.ceramint.2012.08.087

[7] Suja Jose, M. Senthilkumar, K. Elayaraja, M. Haris, Amal George, A. Dhayal Raj, S. John Sundaram, A. K. H. Bashir, M. Maaza, K. Kaviyarasu, Preparation and characterization of Fe doped n-hydroxyapatite for biomedical application, *Surfaces and Interfaces*, 25, (2021), 101185 https://doi.org/10.1016/j.surfin.2021.101185

[8] Anna Tampieri, Teresa D'Alessandro, Monica Sandri, Simone Sprio, Elena Landi, Luca Bertinetti, Silvia Panseri, Giancarlo Pepponi, Joerg Goettlicher, Manuel Bañobre-López, Jose Rivas, Intrinsic magnetism and hyperthermia in bioactive Fe-doped hydroxyapatite, *Acta Biomaterialia*, 8, 2, (2012), 843-851 https://doi.org/10.1016/j.actbio.2011.09.032

[9] Daniela Predoi, Simona Liliana Iconaru, Steluta Carmen Ciobanu, Silviu-Adrian Predoi, Nicolas Buton, Christelle Megier, Mircea Beuran, Development of Iron-Doped Hydroxyapatite Coatings, *Coatings*, 11, 2, (2021), 186 https://doi.org/10.3390/coatings11020186

[10] Negar Alizadeh, Abdollah Salimi, Facile Synthesis of Fe-Doped Hydroxyapatite Nanoparticles from Waste Coal Ash: Fabrication of a Portable Sensor for the Sensitive and Selective Colorimetric Detection of Hydrogen Sulfide, *ACS Omega*, 7, 47, (2022), 42865-42871 https://doi.org/10.1021/acsomega.2c04905

[11] Kaiqian Shu, Chitiphon Chuaicham, Yuto Noguchi, Longhua Xu, Keiko Sasaki, In-situ hydrothermal synthesis of Fe-doped hydroxyapatite photocatalyst derived from converter slag toward xanthate photodegradation and Cr(VI) reduction under visible-light irradiation, *Chemical Engineering Journal*, 459, (2023), 141474 https://doi.org/10.1016/j.cej.2023.141474

[12] N. A. S. Mohd Pu'ad, P. Koshy, H. Z. Abdullah, M. I. Idris, T. C. Lee, Syntheses of hydroxyapatite from natural sources, *Heliyon*, 5, 5, (2019), e01588 https://doi.org/10.1016/j.heliyon.2019.e01588

[13] Ayan K. Barui, Rajesh Kotcherlakota, Chitta R. Patra, Chapter 6 - Biomedical applications of zinc oxide nanoparticles, in: A.M. Grumezescu (Ed.) *Inorganic Frameworks as Smart Nanomedicines*, William Andrew Publishing, 2018, https://doi.org/10.1016/B978-0-12-813661-4.00006-7

[14] Emon Barua, Ashish B. Deoghare, Sushovan Chatterjee, Pranav Sapkal, Effect of ZnO reinforcement on the compressive properties, in vitro bioactivity, biodegradability and cytocompatibility of bone scaffold developed from bovine bone-derived HAp and PMMA, *Ceramics International*, 45, 16, (2019), 20331-20345 https://doi.org/10.1016/j.ceramint.2019.07.006

[15] Vignesh R. Sivaperumal, Rajkumar Mani, Veerababu Polisetti, Kanakaraj Aruchamy, Taehwan Oh, One-Pot Hydrothermal Preparation of Hydroxyapatite/Zinc Oxide Nanorod Nanocomposites and Their Cytotoxicity Evaluation against MG-63 Osteoblast-like Cells, *Molecules*, 28, 1, (2023), 345 https://doi.org/10.3390/molecules28010345

[16] Saryati Saryati, Sulistioso Giat S., Ari Handayani, Supardi Supardi, Puji Untoro, Bambang Sugeng, Hidroksiapatit Berpori dari Kulit Kerang, *Jurnal Sains Materi Indonesia*, 13, 4, (2018), 31-35

[17] Sri Wardhani, Darjito Darjito, Sintesis Hidroksiapatit dari Tulang Sapi dengan Metode Basah-pengendapan, Brawijaya University, 2014

[18] Omer Kaygili, Sergey V. Dorozhkin, Tankut Ates, Ahmed A. Al-Ghamdi, Fahrettin Yakuphanoglu, Dielectric properties of Fe doped hydroxyapatite prepared by sol–gel method, *Ceramics International*, 40, 7, Part A, (2014), 9395-9402 https://doi.org/10.1016/j.ceramint.2014.02.009

[19] Robert D. Shannon, Revised effective ionic radii and systematic studies of interatomic distances in halides and chalcogenides, *Acta crystallographica section A: crystal physics, diffraction, theoretical and general crystallography*, 32, 5, (1976), 751-767 https://doi.org/10.1107/S0567739476001551

[20] P. Scherrer, Bestimmung der inneren Struktur und der Größe von Kolloidteilchen mittels Röntgenstrahlen, in: *Kolloidchemie Ein Lehrbuch*, Springer, Berlin, Heidelberg, 1918, https://doi.org/10.1007/978-3-662-33915-2_7

[21] Hülya Güneş Ateş, Omer Kaygili, Niyazi Bulut, Fatih Osmanlıoğlu, Serhat Keser, Beyhan Tatar, Bahroz Kareem Mahmood, Tankut Ates, Filiz Ercan, Ismail Ercan, Burhan Ates, İmren Özcan, Investigation of the structural, thermal, magnetic and cell viability properties of Ce/Sr co-doped hydroxyapatites, *Journal of Molecular Structure*, 1283, (2023), 135318 https://doi.org/10.1016/j.molstruc.2023.135318

[22] C. C. Silva, I. F. Vasconcelos, A. S. B. Sombra, M. A. Valente, Magnetic properties study on Fe-doped calcium phosphate, *Physica Scripta*, 80, (2009), 055706 https://doi.org/10.1088/0031-8949/80/05/055706

[23] Ram Kishore Singh, M. Srivastava, N. K. Prasad, Sharad Awasthi, Arunkumar Dhayalan, S. Kannan, Iron doped β -Tricalcium phosphate: Synthesis, characterization, hyperthermia effect, biocompatibility and mechanical evaluation, *Materials Science and Engineering: C*, 78, (2017), 715-726 https://doi.org/10.1016/j.msec.2017.04.130